

2020-02-15

# What determines the downstream evolution of turbidity currents

Heerema, C

<http://hdl.handle.net/10026.1/15245>

---

10.1016/j.epsl.2019.116023

Earth and Planetary Science Letters

Elsevier

---

*All content in PEARL is protected by copyright law. Author manuscripts are made available in accordance with publisher policies. Please cite only the published version using the details provided on the item record or document. In the absence of an open licence (e.g. Creative Commons), permissions for further reuse of content should be sought from the publisher or author.*

1 **Title: What determines the downstream evolution of turbidity currents?**

2

3 **Authors**

4 Catharina J. Heerema\*<sup>1</sup>, Peter J. Talling<sup>1</sup>, Matthieu J. Cartigny<sup>1</sup>, Charles K. Paull<sup>2</sup>, Lewis

5 Bailey<sup>3,4</sup>, Stephen M. Simmons<sup>5</sup>, Daniel R. Parsons<sup>5</sup>, Michael A. Clare<sup>4</sup>, Roberto Gwiazda<sup>2</sup>, Eve

6 Lundsten<sup>2</sup>, Krystle Anderson<sup>2</sup>, Katherine L. Maier<sup>2,6,7</sup>, Jingping P. Xu<sup>8,9</sup>, Esther J. Sumner<sup>3</sup>, Kurt

7 Rosenberger<sup>6</sup>, Jenny Gales<sup>10</sup>, Mary McGann<sup>6</sup>, Lionel Carter<sup>11</sup>, Ed Pope<sup>1</sup>, and Monterey

8 Coordinated Canyon Experiment (CCE) Team.

9

10 **Affiliations**

11 <sup>1</sup> Departments of Geography and Earth Sciences, Durham University, Durham, DH1 3LE, U.K.

12 <sup>2</sup> Monterey Bay Aquarium Research Institute, Moss Landing, California 95039, USA.

13 <sup>3</sup> Ocean and Earth Science, University of Southampton, European Way, Southampton, SO14 3ZH,

14 U.K.

15 <sup>4</sup> National Oceanography Centre, University of Southampton Waterfront Campus, European

16 Way, Southampton SO14 3ZH, U.K.

17 <sup>5</sup> Energy and Environment Institute, University of Hull, Cottingham Road, Hull, HU6 7RX, UK.

18 <sup>6</sup> Pacific Coastal and Marine Science Center, U.S. G.S, Santa Cruz, CA 95060, U.S.A.

19 <sup>7</sup> National Institute of Water and Atmospheric Research, Wellington, New Zealand.

20 <sup>8</sup> Southern University of Science and Technology of China, Shenzhen, 518055, China.

21 <sup>9</sup> Qingdao National Laboratory for Marine Science and Technology, Qingdao, 266061, China.

22 <sup>10</sup> University of Plymouth, Drake Circus, Plymouth, PL4 8AA, UK.

23 <sup>11</sup> Antarctic Research Centre, Victoria University of Wellington, Wellington, New Zealand.

24 \*Corresponding author: Catharina Heerema (email: [catharina.j.heerema@durham.ac.uk](mailto:catharina.j.heerema@durham.ac.uk)).

25 ***Abstract:***

26 Seabed sediment flows called turbidity currents form some of the largest sediment accumulations,  
27 deepest canyons and longest channel systems on Earth. Only rivers transport comparable  
28 sediment volumes over such large areas; but there are far fewer measurements from turbidity  
29 currents, ensuring they are much more poorly understood. Turbidity currents differ fundamentally  
30 from rivers, as turbidity currents are driven by the sediment that they suspend. Fast turbidity  
31 currents can pick up sediment, and self-accelerate (ignite); whilst slow flows deposit sediment  
32 and dissipate. Self-acceleration cannot continue indefinitely, and flows might reach a near-  
33 uniform state (autosuspension). Here we show how turbidity currents evolve using the first  
34 detailed measurements from multiple locations along their pathway, which come from Monterey  
35 Canyon offshore California. All flows initially ignite. Typically, initially-faster flows then  
36 achieve near-uniform velocities (autosuspension), whilst slower flows dissipate. Fractional  
37 increases in initial velocity favour much longer runout, and a new model explains this bifurcating  
38 behaviour. However, the only flow during less-stormy summer months is anomalous as it self-  
39 accelerated, which is perhaps due to erosion of surficial-mud layer with fine sands mid-canyon.  
40 Turbidity current evolution is therefore highly sensitive to both initial velocities and seabed  
41 character.

42

43 **Keywords:** Turbidity current; submarine canyon; ignition; dissipation; autosuspension; flow  
44 behaviour

45

## 46 **1. Introduction**

47 Seafloor sediment density flows (called turbidity currents) are the dominant global mechanism  
48 for transporting sediment from the continental shelf to the deep sea. These flows play a crucial  
49 role in global organic carbon burial and geochemical cycles (Galy et al., 2007), and supply of  
50 nutrients to deep-sea ecosystems (Canals et al., 2006). Only rivers transport sediment over  
51 comparable areas, although one turbidity current can carry more sediment than the annual flux  
52 from all the world's rivers combined (Talling et al., 2013). Powerful turbidity currents can badly  
53 damage seafloor infrastructure, including oil and gas pipelines, and telecommunication cable  
54 networks. The latter carry over 95% of global data traffic (Carter et al., 2014), forming the  
55 backbone of the internet and financial markets. Turbidity current deposits host valuable oil and  
56 gas reserves, and form thick sequences of ancient rocks that record Earth's history (Nilsen et al.,  
57 2008). The downstream evolution of velocities and runout lengths controls how sediment is  
58 dispersed, the resulting deposit character and shape, and hazards to seafloor infrastructure. It is  
59 thus important to understand how turbidity currents work, especially what controls their runout,  
60 and changes in flow velocity with distance.

61

62 Turbidity currents differ profoundly from terrestrial rivers; unlike rivers they are driven by the  
63 weight of sediment they carry, and this sediment can be entrained or deposited onto the seafloor  
64 along turbidity current pathways. Previous work suggested that exchange of sediment with the  
65 seabed may lead to positive feedbacks, such that turbidity current behaviour is inherently  
66 unstable and diverges (Fig. 1) (Bagnold, 1962; Parker, 1982). These studies proposed that flows  
67 which erode sediment become denser, and thus accelerate, causing increased erosion, and further  
68 acceleration (Fig. 1a). This process is called ignition, and it may play a pivotal role in producing  
69 powerful and long runout flows. Conversely, flows that deposit sediment may decelerate, leading

70 to further deposition ('dissipation'; Fig. 1b). Such positive feedbacks may produce thresholds in  
71 behaviour that depend on small differences in initial flow state. It has also been proposed that  
72 flows could achieve a near-uniform state in which erosion is balanced by sediment deposition,  
73 termed autosuspension (Fig. 1c, d) (Pantin, 1979). Here, turbulence within the flow is strong  
74 enough to keep particles in suspension, and counteracts their settling velocity (Parker, 1982).  
75 However, unlike ignition, there is no net gain of sediment from the bed, as the bed is too hard to  
76 erode (Fig. 1c), or sediment erosion balances sediment deposition during autosuspension (Fig.  
77 1d). Flows that balance erosion and deposition will tend towards spatially uniform velocities,  
78 assuming that seabed gradient and flow width do not change markedly. Self-acceleration due to  
79 ignition is unlikely to continue indefinitely: increased sediment concentrations will eventually  
80 damp the turbulence that keeps sediment aloft (Baas et al., 2009) and shield the bed from rapid  
81 erosion, or increase frictional drag and thus reduce flow velocities. However, there is  
82 considerable debate over what happens after ignition ceases (Fig. 1a). Do the flows reach a state  
83 of autosuspension; and if so, what do autosuspending flows look like? In particular, do flows  
84 develop a dense near-bed layer that drives the event (as proposed by e.g. Winterwerp, 2006), or  
85 remain an entirely dilute and fully turbulent suspension (e.g. Cantero et al., 2012)?

86  
87 Turbidity currents are notoriously difficult to monitor in action, due to their location, episodic  
88 occurrence, and ability to damage instruments in their path (Inman et al., 1976; Talling et al.,  
89 2013). Consequently, there are very few direct measurements from oceanic turbidity currents,  
90 ensuring fundamental theories on how turbidity currents work are poorly tested. In particular,  
91 ignition and autosuspension have been difficult to reproduce in laboratory experiments (Southard  
92 and Mackintosh, 1981). This may be because most laboratory experiments are relatively slow  
93 moving, compared to full-scale oceanic flows, and thus have limited ability to erode their

94 substrate, or fully support sediment with realistic grain sizes. Experimental flows thus tend to  
95 dissipate. Sequeiros et al. (2009, 2018) successfully produced self-accelerating turbidity currents  
96 in relatively slow moving ( $< 20$  cm/s) laboratory experiments with low density particles, but they  
97 did not reproduce fully realistic processes of seabed erosion. However, new technologies have  
98 recently led to major advances in monitoring of active turbidity currents (Hughes Clarke, 2016).  
99 This includes acoustic Doppler current profilers (ADCPs) that measure velocity profiles to within  
100 a few meters of the seafloor (Xu, 2010). Here we use ADCP and other sensor data to observe  
101 spatial patterns of flow ignition, dissipation, and autosuspension in unprecedented detail; and to  
102 study how flows work in general.

103  
104 This study analyses the most detailed (7 locations at sub-minute intervals) field measurements yet  
105 from oceanic turbidity currents, which include the fastest (up to 7.2 m/s) flows captured via  
106 moored instruments. These measurements come from the upper 52 km of Monterey Canyon,  
107 offshore California (Fig. 2a) (Paull et al., 2018). Previous direct monitoring of turbidity currents  
108 has typically involved measurements at a relatively small number ( $\leq 3$ ) of locations along their  
109 pathway, which provides limited information on how flows behave (Khripounoff et al., 2009; Liu  
110 et al., 2012; Azpiroz-Zabala, 2017). By having measurements in seven locations along a turbidity  
111 current pathway we are able to determine how flows evolve. Here we focus on changes in the  
112 average flow front velocities between measurement locations (termed transit velocities),  
113 maximum internal velocities, as well as duration of flow velocities in each event (as measured by  
114 ADCPs).

115

116 **1.1. Aims**

117 The first aim is to document changes in turbidity current velocity and runout distance, and hence  
118 flow behaviour. What is the observed pattern of ignition, autosuspension and dissipation; and do  
119 multiple flows show a consistent pattern of behaviour? The second aim is to understand what  
120 causes these patterns of flow behaviour. In particular, we consider how two factors (initial  
121 velocity and substrate erodibility) affect flow behaviour, and how near-uniform flow  
122 (autosuspension) may follow ignition. Our third aim is to determine if broadly similar flow  
123 behaviour is seen elsewhere, although suitable field data are sparse. Our fourth aim is to compare  
124 these field observations to most widely accepted theories for ignition and autosuspension. To  
125 what extent do these new field data provide a test of past theories? Finally, we develop a new  
126 generalised model for how turbidity currents in submarine canyons floored by loose sand operate,  
127 which better explains these novel field observations.

128

## 129 **1.2. Terminology**

130 *Turbidity current* is used here as a general term for all types of submarine sediment density flow.  
131 *Dense flow* signifies sediment concentrations that are high enough to damp turbulence  
132 significantly, such that turbulence is no longer the main support mechanism, whilst *dilute flow* is  
133 fully turbulent. There is no single threshold value for sediment concentration at which turbulence  
134 is strongly damped, as this depends on multiple factors including flow velocity, sediment  
135 mineralogy and grain size. But dilute flows typically have sediment concentrations of  $\ll 1\%$ ,  
136 whilst dense flows might often contain  $> 10\%$  sediment by volume. *Diverging* behaviour denotes  
137 how small changes in initial flow velocity are linked to large changes in subsequent runout. It  
138 does not imply that flow behaviour is bimodal, and intermediate runout lengths can still occur.

139

140 **2. Material and Methods**

141 The Coordinated Canyon Experiment (CCE) monitored the upper 50 km of Monterey Canyon  
142 (California, USA) to water depths of 1850 m, for 18 months from 2015 to 2017 (Fig. 2) (Paull et  
143 al., 2018). Sand is primarily delivered to the canyon head via longshore drift, with little river  
144 input (Paull et al., 2005). The entire canyon-channel system extends for over 300 km, but flows  
145 that runout for over 60 km, to a water depth of 2,850 m, only occur every few hundred years  
146 (Stevens et al., 2014). Flows are confined, and experience a constant seafloor gradient and width  
147 in the upper part of Monterey Canyon (Fig. 3). The upper Monterey Canyon, up to 2100 m water  
148 depth, has a sinuosity of 1.9 (Paull et al., 2011). The canyon briefly narrows at a constriction  
149 between 1300 and 1400 m water depth, called the Navy Slump (Figs. 2 and 3) (Paull et al., 2011).  
150 This study uses data recorded by ADCPs along the canyon thalweg (Fig. 2), which were part of a  
151 larger instrumental array (Supplementary fig. 1) (Paull et al., 2018).

152

153 **2.1. ADCP measurements**

154 ADCPs documented velocity profiles through the turbidity currents (Fig. 3; Supplementary Fig.  
155 1), although they are typically unable to make measurements within a few meters of the bed. The  
156 shallowest five mooring stations (MS1 to 5), and deepest mooring station (MS7), had downward-  
157 looking 300 kHz ADCPs located approximately 65 m above the bed seafloor (Paull et al., 2018).  
158 ADCPs on these moorings recorded velocity at 30 second intervals. A Seafloor Instrument Node  
159 (SIN) was located between MS5 and MS7, which contained three separate upward-looking  
160 ADCPs recording at 10 second intervals, using acoustic sources with three different frequencies  
161 (300, 600, 1200 kHz). No reliable ADCP measurements of current velocity are available from the  
162 shallowest mooring (MS1) for some flows, as this mooring broke loose on January 15, 2016  
163 (Paull et al., 2018).



164

## 165 **2.2. Maximum flow velocity measured by ADCPs**

166 Determining the maximum reliable velocity measured by the ADCP is not straightforward. The  
167 arrival of an event is accompanied by mooring tilt and high near-bed sediment concentrations,  
168 influencing the ability of ADCPs to accurately record velocities (Paull et al., 2018). Side-lobe  
169 interference may compromise some ADCP measurements within 1-3 m of the seabed (Teledyne  
170 RD Instruments, 2011), although this depends on the relative strength of backscatter from side-  
171 lobe areas and sediment in the flow. We thus adopted a consistent procedure for calculating  
172 maximum ADCP-measured velocities, which excludes the 20 highest values during an event. The  
173 overall trend of internal velocities remains the same, and therefore our ADCP data processing  
174 does not change this paper's main conclusions.

175

## 176 **2.3. Transit velocities and runout distance**

177 Flow arrival times at the 6 ADCP moorings and SIN were used to measure transit velocities,  
178 which are average front velocities across distances between 0.5 km and 15 km (Fig. 3a). Arrival  
179 times are based on 30 second (or 10 second for SIN) recording interval of the ADCPs, corrected  
180 for clock drift. Distances between sensors were measured along the canyon thalweg, based on a  
181 15 m bathymetric grid. It is assumed that flows principally followed the thalweg (Fig. 2a).

182

## 183 **2.4. Duration of powerful flow measured by ADCPs**

184 As frontal or maximum velocities only tell part of how flow is evolving, and changes in velocity  
185 structure, the duration of a fast-moving flow is also quantified and presented (Table, 1;

186 Supplementary fig. 4). This duration, determined for three different velocity thresholds, provides  
187 an additional indication of how flows may lengthen or stretch over time.

188

## 189 **2.5. Canyon topography**

190 Seafloor gradient is determined along a midline through the canyon thalweg (Fig. 3b), using an  
191 average of 10 grid-cells, each of which has a length of 15 m. Canyon width is defined using the  
192 area of active bedforms (Paull et al., 2018), and measured every 200 m down the canyon. The  
193 canyon floor is delimited by steep canyon walls with slopes of ~10 to 45°.

194

## 195 **2.6. Grain sizes**

196 Sediment traps were mounted at 10 meters above the seafloor on moorings (Supplementary fig.  
197 1). They were tilted and brought closer to the bed by the initial powerful stages of some flows.  
198 Grain sizes in sediment traps from the upper canyon (MS1, MS2, and MS3) were used for most  
199 events. For the September 1<sup>st</sup> event, MS3 and MS4 are used, as the event ignited farther down in  
200 the canyon. Laser particle grain size measurements were taken every 1-5 cm from traps. Discs  
201 released automatically into the traps at 8-day intervals provided time markers. Supplementary fig.  
202 5 shows grain size distribution for the flow events, including mean grain sizes used for Fig. 6.

## 203 **3. Results**

204 The entire sensor array in Monterey Canyon recorded 15 flows (Paull et al., 2018). Here we  
205 consider only the 13 flows measured using the moored ADCP array (Fig. 2b; Supplementary figs.  
206 1 and 2), as we rely on ADCP measurements. Twelve of these 13 ADCP-measured flows started  
207 in the upper canyon at water depths of < 300 m. Flows were measured first by ADCPs at  
208 Mooring Station (MS) 1, located 6.7 km from the canyon head (Figs. 2a and 3a). Many flows

209 then rapidly dissipated, including six flows that died out entirely before MS2, which is 9 km  
210 downstream of MS1 (Fig. 3a). Of the seven flows measured at multiple moorings, three flows  
211 terminated within the sensor array. One event occurred only in the mid-canyon, between MS4  
212 and MS5. Three further flows swept through the entire sensor array, running out for over 50 km  
213 from the canyon head, although they had very different velocities and durations at the final sensor  
214 site (Fig. 4). Most (12 of 13) flows were initiated during the winter months (Fig. 2b), during  
215 which time storm waves are most pronounced and are thought to be important for flow initiation  
216 (Paull et al., 2018). Only one event occurred in the summer months. This event on September 1<sup>st</sup>  
217 2016 did not coincide with large wave heights, a river flood, or earthquake; suggesting another,  
218 as yet poorly understood, trigger (Paull et al., 2018).

219  
220 Transit velocities are available for the seven flows that reached multiple moorings (Fig. 3a). The  
221 transit velocities between the first two moorings (MS1 and MS2) have broadly similar values of  
222 between 4 and 6 m/s. The runout length of these flows varied greatly, with large increases in  
223 runout length correlating with only slightly faster initial frontal velocity (Fig. 3a). However, one  
224 event recorded during the CCE experiment showed a different trend, and it was the only event  
225 occurring outside the winter months, on September 1<sup>st</sup> (Fig. 1b). This event started with an initial  
226 comparatively low frontal velocity between MS1 and MS2 of ~4 m/s, identical to the initial  
227 frontal velocity of the November 24<sup>th</sup> event (Fig. 1c) (Paull et al., 2018). However, the November  
228 24<sup>th</sup> event failed to reach MS3; whilst the September 1<sup>st</sup> event accelerated between MS3 and  
229 MS5, and reached the end of the instrument array (Fig. 3a).

230  
231 The maximum ADCP velocities measured within flows occurred within the first 10 minutes of  
232 the flow front arrival. These internal velocities show a broadly similar pattern to the transit

233 velocities (Fig. 3a). Flows with slower maximum ADCP-measured velocities at the first mooring  
234 tended to die out abruptly in the upper canyon, whilst events with faster ADCP-measured  
235 velocities ran out for much longer distances (Fig. 3a). Note that ADCP measurements define six  
236 shorter runout events that are only recorded at one mooring, and thus lack transit velocity data.

237  
238 Flow behaviour is only partly captured by transit and maximum ADCP measured velocities. For  
239 example, modest increases in transit velocity are often associated with more prolonged periods of  
240 powerful flow (Fig. 4, Table 1). As a powerful flow is more efficient in entraining substrate, the  
241 duration of powerful flow is important for ignition or autosuspension. Flows tend to stretch, as  
242 the frontal part of the flow runs ahead from the slower moving body and tail (Fig. 4) (Azpiroz-  
243 Zabala, 2017). Overall, long run-out events occurring in winter tended to significantly stretch,  
244 such that they extended for almost the entire length of the instrument array. Shorter winter events,  
245 based on data from the shorter winter event on November 24<sup>th</sup>, are initially ~10 km in length as  
246 the event arrives at MS2, but die out in the upper-canyon. The long runout summer event was  
247 initially weak, but became much more prolonged and faster mid-canyon, as well as increasing its  
248 transit velocity; before dissipating rapidly between MS5 and MS7 (Fig. 4). Most flows started  
249 with a flow front thickness <10m. The long run-out events in winter developed thicknesses >30  
250 m (Fig. 4) (Paull et al., 2018).

251

## 252 **4. Discussion**

### 253 ***4.1. Is there a consistent pattern of behaviour for turbidity currents?***

254 Eleven of the twelve flows show a broadly consistent pattern of runout behaviour, which can be  
255 based on the initial transit velocity between the first two moorings, and the maximum ADCP-

256 measured velocities at the first mooring (Fig. 3a). Flows with the fastest initial velocities tend to  
257 run out further. However, small changes in initial transit velocities, or maximum ADCP-  
258 measured velocities, lead to much larger changes in runout distance and subsequent flow  
259 velocity. Runout distances are thus highly sensitive to initial velocities, leading to diverging flow  
260 behaviour (Fig. 3a). All flows initially accelerate, and the initially fastest flows have near-  
261 uniform transit velocities for several tens of kilometres and can stretch up to 35 km in length (4).  
262 Flows with only fractionally slower ( $\sim 0.5$  m/s) initial transit velocities, or maximum ADCP-  
263 measured velocities, die out mid-canyon. The six slowest moving flows at MS1 terminate rapidly  
264 before reaching MS2 (Fig. 3a). These flows that die out in the upper or mid-canyon are initially  
265 powerful, and can sometimes carry heavy (800 kg) objects, or move moorings down-canyon, at  
266 velocities of  $\geq 4$  m/s, but their power does not persist for several kilometres. Only the fastest  
267 flows at the first mooring maintain their velocity for longer distances, and lengthen significantly.  
268 The single exception to this general pattern of behaviour (Figs. 2c and 3) occurred on September  
269 1<sup>st</sup> 2016. This flow's transit velocity and maximum ADCP-measured velocity increased in the  
270 mid-canyon (Fig. 3a), and the duration of powerful flow lengthened markedly (Fig. 4).  
271  
272 These field data thus provide new insights into where and how flows ignite, dissipate or  
273 autosuspend. A notable observation is that the four most powerful flows at MS1 have near-  
274 uniform transit velocities for  $\sim 20$ -35 km, from MS1 to MS3; and near-uniform maximum internal  
275 (ADCP-measured) velocities from MS1 to MS2 (Fig. 3a). This suggests that an initial phase of  
276 acceleration (ignition) is followed by near-uniform flow velocities (autosuspension), at least near  
277 the flow front. Transit velocities are averages over substantial distances, and internal (ADCP-  
278 measured) velocities come from a few specific locations. Thus, it is possible that flow velocities

279 show greater localized variability than depicted in Fig. 3a. However, available field data indicate  
280 near-uniform transit velocities (autosuspension) over substantial distances.

281

#### 282 **4.2. What factors control turbidity current behaviour?**

283 We now seek to understand what controls these patterns of flow behaviour. Twelve flows  
284 accelerated rapidly from rest within the upper 6.7 km of the canyon, reaching velocities of at least  
285 3 to 6 m/s at MS1 (Fig. 2). These turbidity currents were most likely generated by seabed failure,  
286 typically during storm events, as sediment plumes from rivers are weak or absent (Paull et al.,  
287 2018). An initial phase of acceleration will partly result from gravitational acceleration of the  
288 failed mass, but it may also indicate that flows eroded the seabed and self-accelerated (ignited).  
289 However, the relative importance of simple gravitational acceleration of an initial failure, and  
290 ignitive self-acceleration via subsequent seabed erosion, is uncertain due to a lack of repeat  
291 bathymetric surveys with high enough frequency upstream of MS1.

292

293 Beyond MS1, small (< 0.5-1 m/s) increases in initial transit or maximum ADCP-measured  
294 velocities are associated with profound differences in subsequent flow behaviour (Figs. 2c and 3).  
295 We thus infer that initial velocities in the upper canyon determine later flow behaviour. Flows  
296 with only fractionally higher initial transit velocities, or maximum internal ADCP-measured  
297 velocities, tend to run out for much greater distances (Fig. 3a; Table 1). This strongly diverging  
298 flow behaviour is not due to changes in seafloor gradient or canyon width, as canyon axial  
299 channel width (~200 m) and gradient (~ 2°) are relatively uniform from MS1 to MS3 (Fig. 2d, e),  
300 and all of these flows experienced similar changes in canyon slope and width. However, the  
301 axial channel widens significantly beyond MS3 (from ~200 to ~600 m), which may explain why  
302 most flows consistently decelerate beyond MS3 and MS4 (Fig. 3).

303

304 The September 1<sup>st</sup> event is anomalous, as it was initially slow moving but its transit velocity then  
305 increased mid-canyon (Fig. 3a), and the duration of powerful flow velocities increased (Fig. 4;  
306 Table 1). This acceleration is not related to steepening or narrowing of the canyon, and cannot be  
307 explained by a ‘tail wind’ from internal tides (Supplementary Fig. 3). This flow was also the only  
308 event to occur in summer (Fig. 2b). One hypothesis is that self-acceleration of the September 1<sup>st</sup>  
309 event resulted from entrainment of a surficial-mud layer, deposited during less-stormy summer  
310 months. Surficial-mud layers that are 1-12 cm thick occur in the nearby La Jolla Canyon (Paull et  
311 al., 2013), whilst mud layers in cores from MS7 in Monterey Canyon are 1-3 cm thick, with  
312 modal grain sizes of ~50-80  $\mu\text{m}$  (Fig. 8 of Maier et al., 2019). However, it is not clear whether  
313 surficial-mud layers are better developed during summer months, as information from repeat  
314 coring during different seasons is lacking. Moreover, strong (50-80 cm/s) internal tides in  
315 Monterey Canyon rework canyon floor mud throughout the year (Maier et al., 2019). An  
316 alternative hypothesis for mid-canyon ignition of the September 1st event is triggering of a local  
317 substrate failure, forming a knickpoint. Such knickpoints are observed in several places on the  
318 canyon floor, and they have been termed ‘master head scarps’ in past work (Paull et al., 2010).  
319 However, we also lack suitably detailed time-lapse seabed surveys from the mid-canyon to  
320 determine whether a local knickpoint failure occurred.

321

#### 322 ***4.3. Do submarine flows in other locations show similar behaviour?***

323 Having determined that there is a consistent pattern of flow behaviour in Monterey Canyon,  
324 albeit with one exception, we now seek to understand if similar behaviour occurs elsewhere, and  
325 is thus of more general importance. There are few other locations worldwide where the transit or

326 internal velocities of oceanic turbidity currents have been measured at more than 4 locations  
327 along the flow pathway. Indeed, we are aware of only 3 such datasets (Fig. 5).

328  
329 One of these field datasets comes from cable breaks along Gaoping Canyon, offshore Taiwan,  
330 which (unlike Monterey Canyon) is fed by a major river mouth (Fig. 5b) (Gavey et al., 2017).  
331 Seabed gradients along Gaoping Canyon ( $0.3^{\circ}$ - $1.0^{\circ}$ ; Gavey et al., 2017) are somewhat lower than  
332 Monterey Canyon ( $1.6^{\circ}$ -  $2.3^{\circ}$ ; Paull et al., 2011) (Fig 5). Transit velocities in Gaoping Canyon  
333 are nearly constant for  $\sim 100$  km, suggesting that the turbidity currents reach a near-uniform  
334 equilibrium state. This pattern of uniform flow front velocities (autosuspension) is thus not  
335 specific to Monterey Canyon, and it may persist over even longer distances.

336  
337 A second data set comes from a turbidity current that broke submarine cables offshore from the  
338 Grand Banks, Newfoundland, in 1929 (Heezen and Ewing, 1952; Piper et al., 1988). The  
339 turbidity current resulted from extensive but thin (average 5 m) failures on the continental slope,  
340 with  $\sim 185 \text{ km}^3$  of sediment deposited on the Sohm Abyssal Plain (Piper and Aksu, 1987; Piper et  
341 al., 1988). These failures progressively entrained seawater and evolved into debris flows, and  
342 then turbidity currents (Piper et al., 1999). Flow was confined initially within multiple valleys for  
343 the first  $\sim 500$  km of the pathway (Hughes Clarke et al., 1990), where it reached a transit velocity  
344 of 19 m/s on a gradient of  $\sim 0.5^{\circ}$  (Hughes Clarke et al., 1988). This initial phase of the flow  
345 eroded the seabed, and may have ignited; although this is not demonstrated by flow velocities  
346 from cable breaks. Transit velocities then decreased to 6.2 m/s on gradients of  $\sim 0.15$  to  $0.05^{\circ}$ , as  
347 flow became poorly confined, and spread to become several hundred kilometres wide (Fig. 5c;  
348 Heezen and Ewing, 1952; Hughes Clarke, 1988; Hughes Clarke, 1990; Piper and Hundert, 2002).



349 Its transit velocity continuously decreased with distance during these later stages, showing how  
350 reduction in confinement can control flow behaviour, leading to dissipation.

351

#### 352 ***4.4. Comparison of field data to previous theory of autosuspension and ignition***

353 We now compare our new field observations to previous influential theory that predicts when a  
354 submarine turbidity current will autosuspend or ignite (Bagnold, 1962; Pantin, 1979; Parker,  
355 1982; Parker et al., 1986). It is important to understand whether these unusually detailed field  
356 observations can provide a robust test of such theories.

357

##### 358 ***4.4.1. Initial energy-balance theory***

359 Initial work (Bagnold, 1962; Pantin, 1979; Parker, 1982) formulated a theory for whether  
360 turbidity currents autosuspend or ignite that is based on energy losses and gains by the flow. It  
361 was assumed that movement of sediment down-slope results in loss of potential energy, whilst  
362 energy is expended by processes that keep sediment grains aloft. When energy gains equal or  
363 exceed energy losses, the flow can carry all of the sediment it suspends. Then, if the flow can also  
364 erode loose sediment from the bed, it ignites (Fig. 1). However, if no erodible material is  
365 available, the flow autosuspends. Alternatively, if energy losses exceed energy gains, then some  
366 of the suspended sediment will settle out, and the flow will eventually dissipate.

367

368 Equation 1 and figure 6 result from this initial energy-balance theory (Bagnold, 1962; Pantin,  
369 1979; Parker, 1982), as previously depicted by Sequeiros et al. (2009). Figure 6 predicts the  
370 threshold frontal velocity ( $u_h$ ) for ignition, as a function of sediment settling velocity ( $w_s$ ) and  
371 seafloor gradient ( $\beta$ ). The threshold constant for ignition to occur ( $\epsilon$ ), varies between different

372 authors. Bagnold (1962) and Parker (1982) assume that potential energy gain must at least equal  
373 or exceed energy losses ( $\varepsilon \leq 1$ ). In contrast, Pantin (1979) assumes that only a small fraction  
374 ( $\varepsilon \leq 0.01$ ) of potential energy gain will be available to keep sediment aloft, with most potential  
375 energy being dissipated in other ways.

$$\text{Equation (1)} \quad \frac{w_s \cos\beta}{u_h \sin\beta} \leq \varepsilon \begin{cases} \varepsilon = 0.01 & (\text{Pantin, 1979}) \\ \varepsilon = 1 & (\text{Parker, 1982}) \\ \varepsilon = \cos\beta & (\text{Bagnold, 1962}) \end{cases}$$

376  
377 As we use the flow front velocity ( $u_h$ ), we only consider whether ignition or autosuspension  
378 occurs near the flow front. As noted by past authors (e.g. Bagnold, 1962; Pantin, 1979; Parker,  
379 1982; Sequeiros et al., 2009), Equation 1 is a necessary condition for ignition, but it is not a  
380 sufficient condition for ignition; indeed it is rather conservative (Parker et al., 1986). Suitable  
381 sediment must also be available for erosion and incorporation into the flow. This might not be the  
382 case, for example, if the flow was moving over hard bedrock.

383  
384 Measurements from Monterey Canyon can be combined with Equation 1 to compare observed  
385 and predicted flow velocities associated with ignition (Fig. 6). We use a seabed gradient of  $2^\circ$   
386 (Fig. 1e) (Paull et al., 2018), and sediment traps on moorings for grain size distributions for three  
387 separate turbidity currents. The sediment trap closest to the location of ignition in that flow is  
388 used (Fig. 1c), together with the coarsest subsample from each flow deposit in that trap. These  
389 traps were initially suspended 10 m above the bed, but they were sometimes dragged closer to the  
390 bed during the first few minutes of flow (Paull et al., 2018). The method of Ferguson and Church  
391 (2004) is used to estimate settling velocities for individual grains, which assumes that flow is  
392 dilute. Settling velocities could become hindered at higher sediment concentrations.

393

394 Figure 6 shows transit (average frontal) velocities needed for ignition for the grain sizes captured  
395 by traps in the Monterey Canyon flows, for different values of  $\epsilon$  that have been proposed  
396 previously. There is reasonable agreement between our field observations with the approach of  
397 both Parker (1982), and Bagnold (1962). Where flows ignited in Monterey Canyon, grain sizes  
398 observed in sediment traps mainly lie within the field of ignition (Fig. 6). There is poorer  
399 agreement with Pantin (1979), suggesting that potential energy losses do not need to be 100 times  
400 greater than energy losses to keep sediment aloft, and thus for ignition to occur.

401

#### 402 ***4.4.2. Subsequent more complex turbulence energy-balance theory***

403 The simple energy-balance approach summarized by equation 1 (Bagnold, 1962; Pantin, 1979;  
404 Parker, 1982) sets out a necessary condition for autosuspension or ignition. However, flows that  
405 fulfil equation 1 need not ignite, as other conditions are also important. For example, sediment  
406 exchange with the seabed will strongly influence flow density and thus velocity (Parker et al.,  
407 1986; Traer et al., 2012), whilst entrainment of surrounding water will cause momentum to be  
408 lost (Parker et al., 1986).

409

410 Parker et al. (1986) therefore subsequently developed a more advanced and complete theory. This  
411 theory initially comprised three layer-averaged equations based on budgets of fluid (water) mass,  
412 sediment mass and momentum within the flow (Parker et al., 1986). A fourth layer-averaged  
413 equation was then based on budgets of turbulent kinetic energy within the flow, including  
414 turbulence production at the upper and lower flow boundary, dissipation of turbulence due to  
415 viscosity, and work done by turbulence against vertical density gradients (Parker et al., 1986).

416 This approach led to a more complex criterion for ignition (equation 16 of Parker et al. (1986)).  
417 This criterion involves layer-averaged sediment concentration, flow velocity and thickness,  
418 sediment settling velocity, bed shear velocity, and rates of sediment and water entrainment  
419 (Parker et al., 1986). This more advanced but complex criterion for ignition implicitly assumes  
420 that sediment is mainly supported by fluid turbulence. It would not apply to denser sediment  
421 flows in which turbulence is strongly damped, and where other processes become important for  
422 sediment support, such as support via grain-to-grain collisions, or excess pore pressure.

423

#### 424 ***4.5. Why past autosuspension and ignition theory is difficult to test***

425 Although unprecedented in their detail, our field observations from Monterey Canyon provide a  
426 rather weak test of the initial simpler energy-balance theory (Bagnold, 1962; Pantin, 1979;  
427 Parker, 1982), and they are unable to test the more complex turbulent energy-balance (Parker et  
428 al., 1986) theory, for three key reasons.

429

430 First, both types of theory involve a single sediment settling velocity, and thus require that a  
431 representative grain size is chosen. However, turbidity currents in Monterey Canyon contain a  
432 wide range of grain sizes (Fig. 6), as is often the case for turbidity currents elsewhere. Thus, there  
433 is an issue of which representative grain size to choose from this wide distribution (Fig. 6). There  
434 are also major issues related to measurement of grain size in the field via sediment traps, as traps  
435 only sample grain size at a single height, and traps may be less effective at capturing finer grains  
436 than coarser grains.

437

438 Second, in the case of theory based on turbulent kinetic energy budgets (Parker et al., 1986), we  
439 lack sufficiently precise measurements of key parameters needed by this theory, most notably  
440 layer-averaged sediment concentrations, but also rates of sediment and water entrainment.

441  
442 Finally, and most importantly, some key assumption that underpin past theories may not hold.  
443 For example, Parker's later theory based on turbulent kinetic energy budgets assumes that flow is  
444 dilute, such that turbulence is always the main support mechanism (Parker et al., 1986). Field  
445 evidence suggests that some turbidity currents in Monterey Canyon are driven by dense near-bed  
446 layers with high ( $> 10\%$  by volume) sediment concentrations (Fig. 6) (Paull et al., 2018). These  
447 dense layers are needed to explain the fast ( $\geq 4$  m/s) movement of very heavy (up to 800 kg)  
448 objects for several kilometres (Paull et al., 2018). It is unlikely that entirely dilute flows could  
449 carry such heavy objects, at high velocities, for such distances; the heavy objects are instead  
450 entombed in a dense near-bed layer (Paull et al., 2018). Turbulence is damped strongly in such  
451 dense near-bed layers, and settling will be hindered (Winterwerp, 2006). Other sediment support  
452 mechanisms become important, such as grain collisions or excess pore pressures that partly carry  
453 the sediment load. The more advanced ignition theory (Parker et al., 1986) would thus be unable  
454 to capture the behaviour of flows in Monterey Canyon with dense near-bed layers.

455

#### 456 ***4.6. New travelling wave model***

457 We now outline a new conceptual model for how initially fast moving turbidity currents operate  
458 in confined settings, underlain by loose sand, based on our field observations. Following Paull et  
459 al. (2018), this model includes dense near-bed layers that drive the flow, in which turbulence is  
460 not the main support mechanism. The model thus better fits detailed field observations from

461 Monterey Canyon. A new model is needed because past theory for ignition and autosuspension  
462 (Parker et al., 1986) was not formulated to include dense near-bed layers. The new model differs  
463 from past work (e.g. Paull et al., 2018), as it explains how flows that initially ignite may then  
464 autosuspend, as they reach a uniform transit velocity.

465  
466 We propose that during initial ignition, and the following near-equilibrium (autosuspension)  
467 phase, a fast and dense near-bed layer exists at the flow front, which drives the overall event,  
468 similar to Fig. 7 (Winterwerp, 2006). This dense near-bed layer near the flow front maintains an  
469 approximately uniform frontal velocity, as erosion of the bed near its front, is balanced by  
470 deposition at its rear (Fig. 7). Thus, although the dense layer is locally either erosive or  
471 depositional at a single location, erosion and deposition are balanced over the whole of the layer,  
472 such that the dense layer velocity is near-uniform. This leads to autosuspension (Fig. 7). We  
473 envisage that sediment concentrations in the dense layer (10-30%) are those attributed by  
474 Winterwerp et al. (1992) to hyperconcentrated flow, which is capable of forming the crescentic  
475 shaped bedforms seen along the floor of Monterey Canyon (Winterwerp et al., 1992; Paull et al.,  
476 2018). It has been suggested that liquefied flows of sand could only travel for short distances  
477 (Lowe, 1976) on steep slopes ( $>3^\circ$ ) due to rapid dissipation of excess pore fluid pressures and  
478 basal sedimentation. However, addition of small fractions of cohesive mud, as seen in Monterey  
479 Canyon (Maier et al., 2019), increase the time taken for excess pore pressure to dissipate by  
480 orders of magnitude and hinders settling (Iverson et al., 2010), thus greatly increasing runout of  
481 partly-liquefied flow. Sediment from the dense layer is shed backwards into a dilute and fully  
482 turbulent sediment cloud. This trailing cloud increases in length (stretches) as the dense flow  
483 front runs ahead of the trailing body (Figs. 3 and 6) (Azpiroz-Zabala et al., 2017).

484

485 We term this new model the ‘travelling wave model’, and it is broadly comparable to behaviour  
486 seen in laboratory experiments involving dense, dry granular avalanches (Supplementary fig. 6)  
487 (Pouliquen and Forterre, 2002; Mangeney et al., 2007). A key feature of these experiments is that  
488 the dry avalanches that are fast enough can erode their underlying substrate, in their case loose  
489 sand. These dry granular avalanche experiments show two types of behaviour (Pouliquen and  
490 Forterre, 2002; Mangeney et al., 2007). Slower moving avalanches dissipate, as they fail to erode  
491 and entrain their substrate. However, sufficiently fast moving dry granular avalanches erode, and  
492 form a travelling wave with near-uniform frontal transit velocities (Supplementary fig. 6)  
493 (Pouliquen and Forterre, 2002; Mangeney et al., 2007; Edwards and Gray, 2015). Erosion of sand  
494 from near the front of the travelling wave is balanced by deposition from its rear (Fig. 7). The  
495 avalanche thus contains a substantial fraction of locally eroded material. The transit velocity of  
496 this travelling wave is strongly determined by the thickness of the frontal avalanche, as in the dry  
497 granular experiments (Pouliquen and Forterre, 2002; Mangeney et al., 2007). Frontal thickness  
498 determines the down-slope driving force near the front, at least for near-uniform gradients and  
499 flow densities. The flow thickness in turn depends on the depth of eroded material, and thus on  
500 rates of frontal erosion (Pouliquen and Forterre, 2002; Mangeney et al., 2007). Turbidity currents  
501 will differ in key regards from these dry granular avalanches that occur on far steeper ( $> 30^\circ$ )  
502 gradients. For example, erosion of water-saturated canyon floor sediment, such as via abrupt  
503 loading and liquefaction, may allow turbidity currents to erode on much lower ( $< 2^\circ$ ) gradients  
504 than dry granular avalanches. Settling velocities will be much greater in air, and turbidity currents  
505 can also comprise trailing dilute suspensions. However, we draw a first-order analogy with the  
506 ability of faster moving dry granular avalanches that exceed a threshold and erode their substrate,  
507 whilst depositing from their rear, and thus maintain dense flow with near-uniform transit velocity.  
508

509 This new travelling wave model also needs to account for crescent shaped bedforms that are  
510 abundant along the floor of Monterey Canyon (Paull et al., 2018), and many other sandy  
511 submarine canyons (Symons et al., 2016), which have been linked to instabilities (termed cyclic  
512 steps) in supercritical flows (Hughes Clarke, 2016). Bedforms in Monterey Canyon have  
513 amplitudes of 1 to 3 m, and wavelengths of 20 to 80 m (Paull et al. 2018). As discussed in more  
514 detail by Paull et al. (2018), tracking of extremely heavy (800 kg) objects showed that they  
515 experienced repeated vertical oscillations of 1-3 m, as they were carried down Monterey Canyon  
516 at velocities of ~4 m/s. Bedforms were thus most likely continuously present, and must have been  
517 at least partly formed by the dense travelling wave. This is consistent with field observations and  
518 laboratory experiments showing that cyclic steps and up-slope migrating bedforms can form  
519 beneath supercritical flows with very high (20-40% volume) sediment concentrations  
520 (Winterwerp et al., 1990, 1992) as well as dilute supercritical flows (Kostic and Parker, 2006;  
521 Covault et al., 2017).

522 Future work is now needed to test this new travelling wave model, such as via direct  
523 measurements of sediment concentration in turbidity currents, or by determining the importance  
524 of locally derived or far-travelled sediment in near-bed layers.

525

## 526 **5. Conclusions**

527 Here we analyse the most detailed measurements yet from within seafloor turbidity currents,  
528 showing how their transit and maximum measured internal velocities vary with distance.

529

530 Overall, we observed that small ( $< 0.5$ -1 m/s) increases in average transit velocities are associated  
531 with large differences in subsequent runout (Fig. 8). Fractional increases in initial velocities may



532 lead to flows with near-uniform velocities associated with autosuspension, enabling much longer  
533 runout. Flows with only slightly lower initial velocities die out in upper or mid-canyon. Patterns  
534 of transit and internal velocities with distance thus diverge markedly (Fig. 8).

535  
536 However, one flow in Monterey Canyon is an exception to this general pattern, as it self-  
537 accelerated mid-canyon (Fig. 8, dotted green line). It is also the only flow that occurred during  
538 less-stormy summer months. Erosion of a weak surficial-mud layer with underlying fine sand, is  
539 likely to also favour self-acceleration. Turbidity current behaviour may therefore be highly  
540 sensitive to both initial transit velocities and substrate character.

541  
542 Our observations show that initial self-acceleration (ignition) can be followed by a phase of near-  
543 uniform transit velocities (autosuspension), at least for initially faster flow events (Fig. 8).  
544 Previous models have proposed that autosuspension may follow on from ignition, as erodible bed  
545 material runs out. But this is not the case in Monterey Canyon, as loose sand is available along  
546 the canyon floor. Instead, we propose that flows are driven by thin and dense, frontal, near-bed  
547 layers (which we call a travelling wave; Fig. 7). Faster moving travelling waves can reach an  
548 autosuspending state, as frontal erosion balances deposition from their rear, so that near-uniform  
549 frontal flow thicknesses and thus velocities are maintained. These dense travelling waves shed a  
550 slower moving dilute sediment cloud, which lengthens as the flow runs out. But this dilute cloud  
551 does not drive the flow, and changes in its sediment concentration are thus less important. This  
552 travelling wave model itself needs further testing, including via direct measurements of near-bed  
553 sediment concentrations, but it is consistent with movement of very heavy objects at high  
554 velocity near the flow front (Paull et al., 2018).

555

556 **Acknowledgments**

557 C.J. Heerema is funded by the European Union's Horizon 2020 research and innovation program  
558 under the Marie Skłodowska-Curie grant agreement No 721403 - ITN SLATE. This project  
559 received funding from the David and Lucile Packard Foundation, Natural Environment Research  
560 Council (grant NE/K011480/1), U.S. Geological Survey (USGS) Coastal and Marine Program,  
561 and Ocean University of China. We acknowledge NERC funding (NE/K011480/1,  
562 NE/M007138/1, NE/M017540/1, NE/P009190/1, and NE/P005780/1). M.A. Clare acknowledges  
563 support from NERC National Capability project Climate Linked Atlantic Sector Science  
564 (NE/R015953/1). E. Pope was supported by a Leverhulme Trust Early Career Fellowship (ECF-  
565 2018-267).

566

567 **Data and materials availability**

568 Data are available at <https://doi.org/10.1594/IEDA/324529>.

569

570

571

572

573 **References**

574 Azpiroz-Zabala, M., Cartigny, M.J.B., Talling, P.J., Parsons, D.R., Sumner, E.J., Clare, M.A., Simmons, S.M.,  
575 Cooper, C., Pope, E.L., 2017. Newly recognized turbidity current structure can explain prolonged  
576 flushing of submarine canyons. *Science Advances* 3, e1700200.  
577 <https://doi.org/10.1126/sciadv.1700200>

578 Baas, J.H., Best, J.L., Peakall, J., Wang, M., 2009. A Phase Diagram for Turbulent, Transitional, and  
579 Laminar Clay Suspension Flows. *Journal of Sedimentary Research* 79, 162–183.  
580 <https://doi.org/10.2110/jsr.2009.025>

581 Bagnold, R.A., 1962. Auto-suspension of transported sediment; turbidity currents. *Proceedings of the*  
582 *Royal Society of London* 265, 315–319. <https://doi.org/10.1098/rspa.1962.0012>

583 Canals, M., Puig, P., Madron, X.D. de, Heussner, S., Palanques, A., Fabres, J., 2006. Flushing submarine  
584 canyons. *Nature* 444, 354–357. <https://doi.org/10.1038/nature05271>

585 Cantero, M.I., Cantelli, A., Pirmez, C., Balachandar, S., Mohrig, D., Hickson, T.A., Yeh, T., Naruse, H.,  
586 Parker, G., 2012. Emplacement of massive turbidites linked to extinction of turbulence in  
587 turbidity currents. *Nature Geoscience* 5, 42–45. <https://doi.org/10.1038/ngeo1320>

588 Carter, L., Gavey, R., Talling, P., Liu, J., 2014. Insights into Submarine Geohazards from Breaks in Subsea  
589 Telecommunication Cables. *Oceanography* 27, 58–67. <https://doi.org/10.5670/oceanog.2014.40>

590 Edwards, A.N., Gray, J.M.N.T., 2015. Erosion–deposition waves in shallow granular free-surface flows.  
591 *Journal of Fluid Mechanics* 762, 35–67. <https://doi.org/10.1017/jfm.2014.643>

592 Ferguson, R.I., Church, M., 2004. A Simple Universal Equation for Grain Settling Velocity. *Journal of*  
593 *Sedimentary Research* 74, 933–937. <https://doi.org/10.1306/051204740933>

594 Galy, V., France-Lanord, C., Beyssac, O., Faure, P., Kudrass, H., Palhol, F., 2007. Efficient organic carbon  
595 burial in the Bengal fan sustained by the Himalayan erosional system. *Nature* 450, 407–410.  
596 <https://doi.org/10.1038/nature06273>

597 Gavey, R., Carter, L., Liu, J.T., Talling, P.J., Hsu, R., Pope, E., Evans, G., 2017. Frequent sediment density  
598 flows during 2006 to 2015, triggered by competing seismic and weather events: Observations

599 from subsea cable breaks off southern Taiwan. *Marine Geology* 384, 147–158.  
600 <https://doi.org/10.1016/j.margeo.2016.06.001>

601 Gladstone, C., Sparks, R.S.J., 2002. The Significance of Grain-Size Breaks in Turbidites and Pyroclastic  
602 Density Current Deposits. *Journal of Sedimentary Research* 72, 182–191.  
603 <https://doi.org/10.1306/041801720182>

604 Heezen, B.C., Ewing, W.M., 1952. Turbidity currents and submarine slumps, and the 1929 Grand Banks  
605 [Newfoundland] earthquake. *American Journal of Science* 250, 849–873.  
606 <https://doi.org/10.2475/ajs.250.12.849>

607 Hughes Clarke, J.E., 1988. The geological record of the 1929 Grand Banks earthquake and its relevance to  
608 deep-sea clastic sediment. Dalhousie University, Nova Scotia, Canada. 171 pp.

609 Hughes Clarke, J.E., 2016. First wide-angle view of channelized turbidity currents links migrating cyclic  
610 steps to flow characteristics. *Nature Communications* 7, 11896.  
611 <https://doi.org/10.1038/ncomms11896>

612 Hughes Clarke, J.E., Shor, A.N., Piper, D.J.W., Mayer, L.A., 1990. Large-scale current-induced erosion and  
613 deposition in the path of the 1929 Grand Banks turbidity current. *Sedimentology* 37, 613–629.  
614 <https://doi.org/10.1111/j.1365-3091.1990.tb00625.x>

615 Inman, D.L., Nordstrom, C.E., Flick, R.E., 1976. Currents in Submarine Canyons: An Air-Sea-Land  
616 Interaction. *Annual Review of Fluid Mechanics* 8, 275–310.  
617 <https://doi.org/10.1146/annurev.fl.08.010176.001423>

618 Iverson, R.M., Logan, M., LaHusen, R.G., Berti, M., 2010. The perfect debris flow? Aggregated results  
619 from 28 largescale experiments *J. Geophys. Res.*, 115, Art. No. F03005.  
620 <https://doi.org/10.1029/2009JF001514>

621 Khripounoff, A., Vangriesheim, A., Crassous, P., Etoubleau, J., 2009. High frequency of sediment gravity  
622 flow events in the Var submarine canyon (Mediterranean Sea). *Marine Geology* 263, 1–6.  
623 <https://doi.org/10.1016/j.margeo.2009.03.014>

624 Liu, J.T., Wang, Y.-H., Yang, R.J., Hsu, R.T., Kao, S.-J., Lin, H.-L., Kuo, F.H., 2012. Cyclone-induced  
625 hyperpycnal turbidity currents in a submarine canyon. *Journal of Geophysical Research: Oceans*  
626 117, C04033. <https://doi.org/10.1029/2011JC007630>

627 Lowe, D.R., 1976. Subaqueous liquefied and fluidised sediment flows and their deposits. *Sedimentology*,  
628 23, 285–308. <https://doi.org/10.1111/j.1365-3091.1976.tb00051.x>

629 Maier, K.L., Gales, J.A., Paull, C.K., Rosenberger, K., Talling, P.J., Simmons, S.M., Gwiazda, R., McGann, M.,  
630 Cartigny, M.J.B., Lundsten, E., Anderson, K., Clare, M.A., Xu, J., Parsons, D., Barry, J.P., Wolfson-  
631 Schwehr, M., Nieminski, N.M., Sumner, E.J., 2019. Linking Direct Measurements of Turbidity  
632 Currents to Submarine Canyon-Floor Deposits. *Front. Earth Sci.* 7, 144.  
633 <https://doi.org/10.3389/feart.2019.00144>

634 Mangeney, A., Tsimring, L.S., Volfson, D., Aranson, I.S., Bouchut, F., 2007. Avalanche mobility induced by  
635 the presence of an erodible bed and associated entrainment. *Geophysical Research Letters* 34,  
636 L22401. <https://doi.org/10.1029/2007GL031348>

637 Nilsen, T.H., Shew, R.D., Steffens, G.S., Studlick, J.R.J. (Eds.), 2008. *Atlas of Deep-Water Outcrops*.  
638 American Association of Petroleum Geologists, Oklahoma, U.S.A.  
639 <https://doi.org/10.1306/St561240>

640 Pantin, H.M., 1979. Interaction between velocity and effective density in turbidity flow: Phase-plane  
641 analysis, with criteria for autosuspension. *Marine Geology* 31, 59–99.  
642 [https://doi.org/10.1016/0025-3227\(79\)90057-4](https://doi.org/10.1016/0025-3227(79)90057-4)

643 Parker, G., 1982. Conditions for the ignition of catastrophically erosive turbidity currents. *Marine*  
644 *Geology* 46, 307–327. [https://doi.org/10.1016/0025-3227\(82\)90086-X](https://doi.org/10.1016/0025-3227(82)90086-X)

645 Parker, G., Fukushima, Y., Pantin, H.M., 1986. Self-accelerating turbidity currents. *Journal of Fluid*  
646 *Mechanics* 171, 145. <https://doi.org/10.1017/S0022112086001404>

647 Paull, C.K., Caress, D.W., Lundsten, E., Gwiazda, R., Anderson, K., McGann, M., Conrad, J., Edwards, B.,  
648 Sumner, E.J., 2013. Anatomy of the La Jolla Submarine Canyon system; offshore southern  
649 California. *Marine Geology* 335, 16–34. <https://doi.org/10.1016/j.margeo.2012.10.003>

650 Paull, C.K., Caress, D.W., Ussler, W., Lundsten, E., Meiner-Johnson, M., 2011. High-resolution bathymetry  
651 of the axial channels within Monterey and Soquel submarine canyons, offshore central  
652 California. *Geosphere* 7, 1077–1101. <https://doi.org/10.1130/GES00636.1>

653 Paull, C.K., Mitts, P., Ussler III, W., Keaten, R., Greene, H.G., 2005. Trail of sand in upper Monterey  
654 Canyon: offshore California. *Geological Society of America Bulletin* 117, 1134–1145.

655 Paull, C.K., Talling, P.J., Maier, K.L., Parsons, D., Xu, J., Caress, D.W., Gwiazda, R., Lundsten, E.M.,  
656 Anderson, K., Barry, J.P., Chaffey, M., O'Reilly, T., Rosenberger, K.J., Gales, J.A., Kieft, B., McGann,  
657 M., Simmons, S.M., McCann, M., Sumner, E.J., Clare, M.A., Cartigny, M.J., 2018. Powerful  
658 turbidity currents driven by dense basal layers. *Nature Communications* 9, 4114.  
659 <https://doi.org/10.1038/s41467-018-06254-6>

660 Paull, C.K., Ussler III, W., Caress, D.W., Lundsten, E., Covault, J.A., Maier, K.L., Xu, J., Augenstein, S., 2010.  
661 Origins of large crescent-shaped bedforms within the axial channel of Monterey Canyon,  
662 offshore California. *Geosphere* 6, 755–774. <https://doi.org/10.1130/GES00527.1>

663 Piper, D.J.W., Aksu, A.E., 1987. The source and origin of the 1929 grand banks turbidity current inferred  
664 from sediment budgets. *Geo-Marine Letters* 7, 177–182. <https://doi.org/10.1007/BF02242769>

665 Piper, D.J.W., Cochonat, P., Morrison, M.L., 1999. The sequence of events around the epicentre of the  
666 1929 Grand Banks earthquake: initiation of debris flows and turbidity current inferred from  
667 sidescan sonar. *Sedimentology* 46, 79–97. <https://doi.org/10.1046/j.1365-3091.1999.00204.x>

668 Piper, D., Hundert, T., 2002. Provenance of distal Sohm Abyssal Plain sediments: history of supply from  
669 the Wisconsinan glaciation in eastern Canada. *Geo-Marine Letters* 22, 75–85.  
670 <https://doi.org/10.1007/s00367-002-0101-2>

671 Piper, D.J.W., Shor, A.N., Hughes Clarke, J.E., 1988. The 1929 “Grand Banks” earthquake, slump, and  
672 turbidity current, in: *Geological Society of America Special Papers*. Geological Society of America,  
673 pp. 77–92. <https://doi.org/10.1130/SPE229-p77>

674 Pouliquen, O., Forterre, Y., 2002. Friction law for dense granular flows: application to the motion of a  
675 mass down a rough inclined plane. *Journal of Fluid Mechanics* 453, 133–151.  
676 <https://doi.org/10.1017/S0022112001006796>

677 Salaheldin, T.M., Imran, J., Chaudhry, M.H., Reed, C., 2000. Role of fine-grained sediment in turbidity  
678 current flow dynamics and resulting deposits. *Marine Geology* 171, 21–38.  
679 [https://doi.org/10.1016/S0025-3227\(00\)00114-6](https://doi.org/10.1016/S0025-3227(00)00114-6)

680 Sequeiros, O.E., Mosquera, R., Pedocchi, F., 2018. Internal Structure of a Self-Accelerating Turbidity  
681 Current. *Journal of Geophysical Research: Oceans* 123, 6260–6276.  
682 <https://doi.org/10.1029/2018JC014061>

683 Sequeiros, O.E., Naruse, H., Endo, N., Garcia, M.H., Parker, G., 2009. Experimental study on self-  
684 accelerating turbidity currents. *Journal of Geophysical Research* 114.  
685 <https://doi.org/10.1029/2008JC005149>

686 Southard, J.B., Mackintosh, M.E., 1981. Experimental test of autosuspension. *Earth Surface Processes*  
687 and *Landforms* 6, 103–111. <https://doi.org/10.1002/esp.3290060204>

688 Stevens, T., Paull, C.K., Ussler, W., McGann, M., Buylaert, J.-P., Lundsten, E., 2014. The timing of  
689 sediment transport down Monterey Submarine Canyon, offshore California. *Geological Society of*  
690 *America Bulletin* 126, 103–121. <https://doi.org/10.1130/B30931.1>

691 Stevenson, C.J., Feldens, P., Georgiopoulou, A., Schönke, M., Krastel, S., Piper, D.J.W., Lindhorst, K.,  
692 Mosher, D., 2018. Reconstructing the sediment concentration of a giant submarine gravity flow.  
693 *Nat Commun* 9, 2616. <https://doi.org/10.1038/s41467-018-05042-6>

694 Symons, W.O., Sumner, E.J., Talling, P.J., Cartigny, M.J.B., Clare, M.A., 2016. Large-scale sediment waves  
695 and scours on the modern seafloor and their implications for the prevalence of supercritical  
696 flows. *Marine Geology* 371, 130–148. <https://doi.org/10.1016/j.margeo.2015.11.009>

697 Talling, P.J., Paull, C.K., Piper, D.J.W., 2013. How are subaqueous sediment density flows triggered, what  
698 is their internal structure and how does it evolve? Direct observations from monitoring of active  
699 flows. *Earth-Science Reviews* 125, 244–287. <https://doi.org/10.1016/j.earscirev.2013.07.005>

700 Teledyne RD Instruments, 2011. Acoustic Doppler Current Profiler principles of operation: a practical  
701 primer. P/N 951-6069-00. RD Instruments, San Diego, CA.

702 Traer, M.M., Hilley, G.E., Fildani, A., McHargue, T., 2012. The sensitivity of turbidity currents to mass and  
703 momentum exchanges between these underflows and their surroundings. *Journal of Geophysical*  
704 *Research: Earth Surface* 117, F01009. <https://doi.org/10.1029/2011JF001990>

705 Winterwerp, J.C., 2006. Stratification effects by fine suspended sediment at low, medium, and very high  
706 concentrations. *Journal of Geophysical Research* 111. <https://doi.org/10.1029/2005JC003019>



707 Winterwerp, J.C., Bakker, W.T., Mastbergen, D.R., van Rossum, H., 1992. Hyperconcentrated Sand-Water  
708 Mixture Flows over Erodible Bed. *Journal of Hydraulic Engineering* 118, 1508–1525.  
709 [https://doi.org/10.1061/\(ASCE\)0733-9429\(1992\)118:11\(1508\)](https://doi.org/10.1061/(ASCE)0733-9429(1992)118:11(1508))

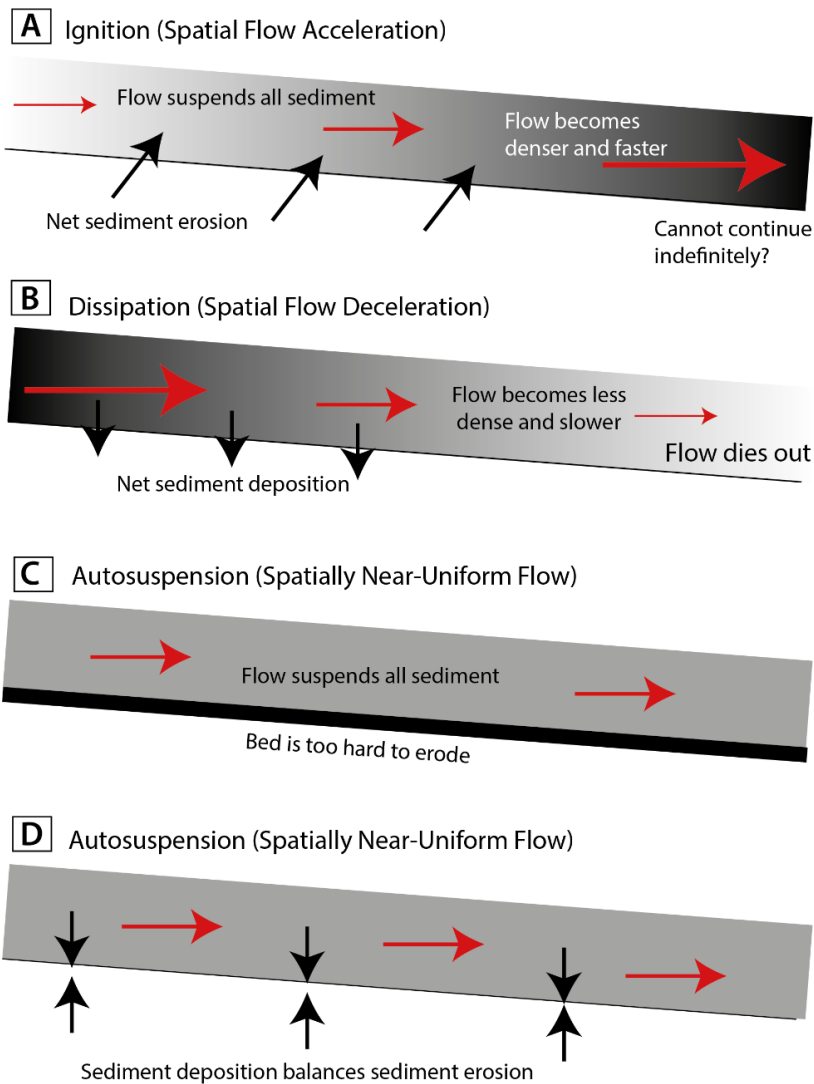
710 Winterwerp, J.C., de Groot, M.B., Mastbergen, D.R., Verwoert, H., 1990. Hyperconcentrated Sand-Water  
711 Mixture Flows Over a Flat Bed. *Journal of Hydraulic Engineering* 116, 36–54.  
712 [https://doi.org/10.1061/\(ASCE\)0733-9429\(1990\)116:1\(36\)](https://doi.org/10.1061/(ASCE)0733-9429(1990)116:1(36))

713 Xu, J.P., 2010. Normalized velocity profiles of field-measured turbidity currents. *Geology* 38, 563–566.  
714 <https://doi.org/10.1130/G30582.1>

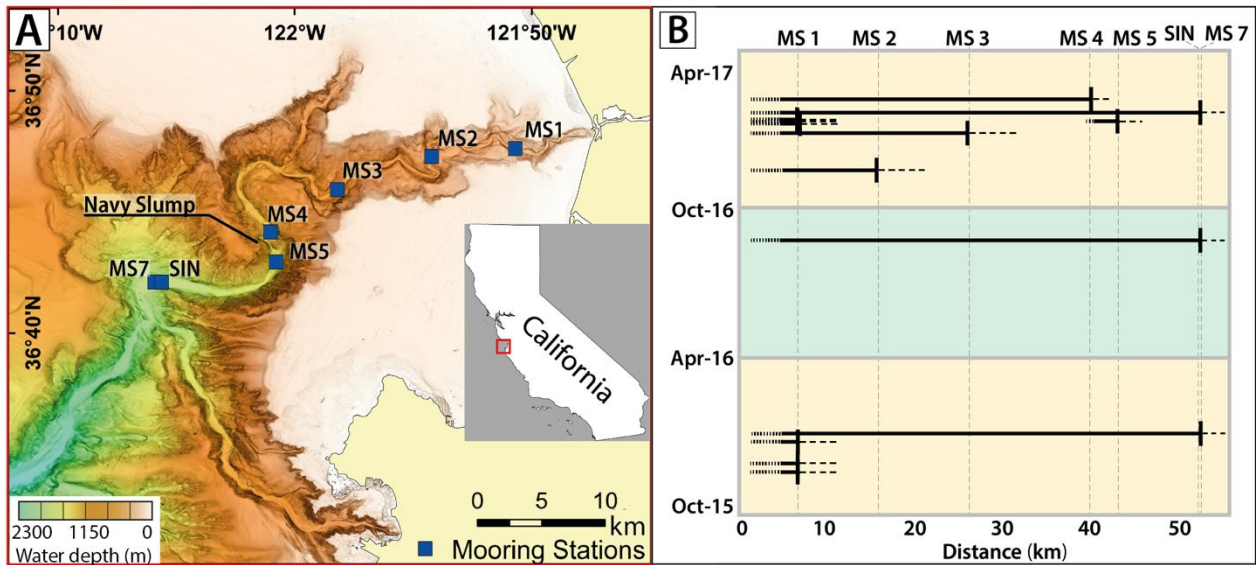
715

716

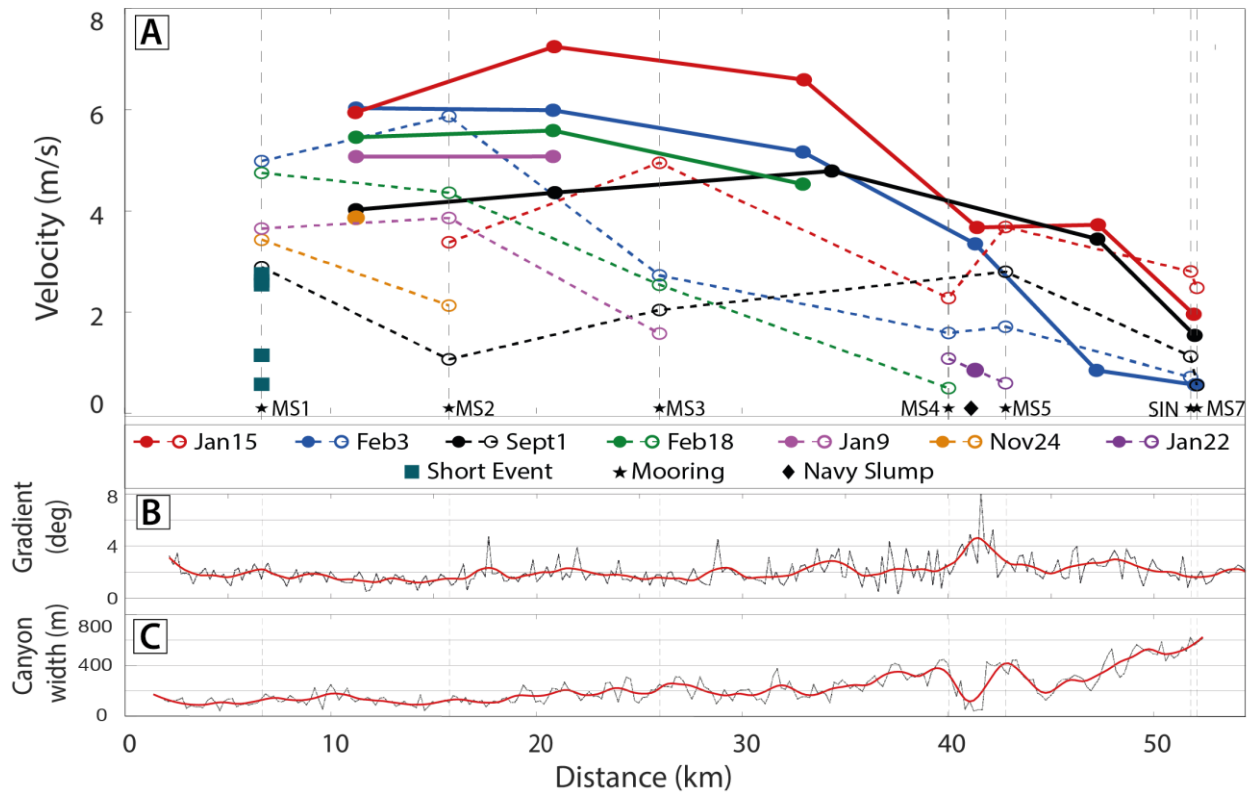
717



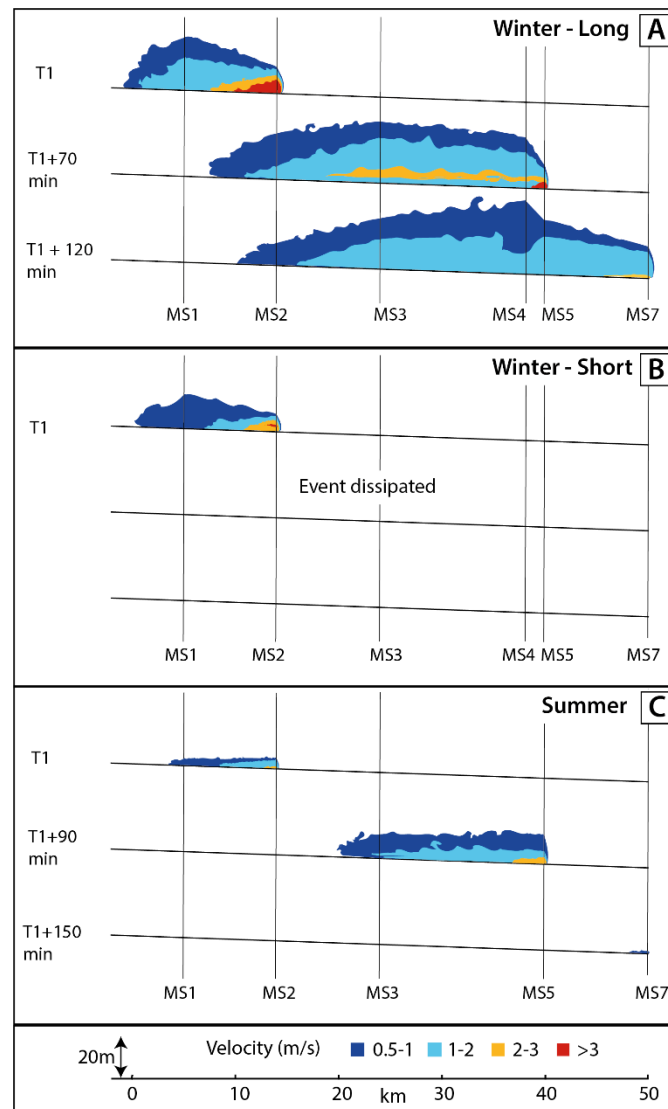
720 **Figure 1. Ignition, dissipation and autosuspension of turbidity currents.** (A) Ignition is  
 721 caused by net sediment erosion that increases flow density, causing increased velocities. This  
 722 positive feedback cannot continue indefinitely, as elevated sediment concentrations eventually  
 723 damp turbulence, shield the bed from erosion, or increase friction. (B) Dissipation is caused by  
 724 sediment deposition, which leads to spatial decreases in flow density, and thus velocity. This  
 725 negative feedback causes the flow to eventually die out. (C and D) Autosuspension comprises a  
 726 situation in which flow density remains constant, and flow velocities are constant spatially. (C)  
 727 Flow may be powerful enough to suspend all of the sediment it carries, but the substrate is too  
 728 hard to erode. Alternatively, localised areas of erosion and deposition may also balance each  
 729 other out, leading to no net change in suspended sediment. (D) Sediment deposition may be  
 730 balanced by an equal amount of substrate erosion. Models for autosuspension in (C) and (D)  
 731 assume flow is dilute and fully turbulent. We subsequently present an alternative model for  
 732 autosuspension (Fig. 7), where flow is driven by a dense near-bed layer.



733  
 734  
 735 **Fig. 2. Location, runout distances and velocities of turbidity currents in Monterey Canyon.**  
 736 (A) Bathymetry map of Monterey Canyon showing location of moorings in this study (MS1 to  
 737 MS7, SIN), and Navy Slump. (B) Timing and runout distance of turbidity currents in Monterey  
 738 Canyon between October 2015 and April 2017. Horizontal lines show 13 events registered by  
 739 ADCPs. The green and yellow boxes show the 6-month deployment periods. Locations of  
 740 moorings (MS1 to MS7, SIN) are indicated. The exact point where flows terminate between  
 741 moorings is uncertain. (C) Changes in flow velocity with distance along Monterey Canyon's  
 742 thalweg. Solid dots and solid lines show frontal velocities between moorings. Open symbols and  
 743 dotted lines show maximum internal velocity measured at each mooring by an ADCP, including  
 744 for some flows that only reached the first mooring (solid squares). (D) Changes in thalweg  
 745 gradient. (E) Changes in axial channel width, defined by the width of mapped bedforms.  
 746

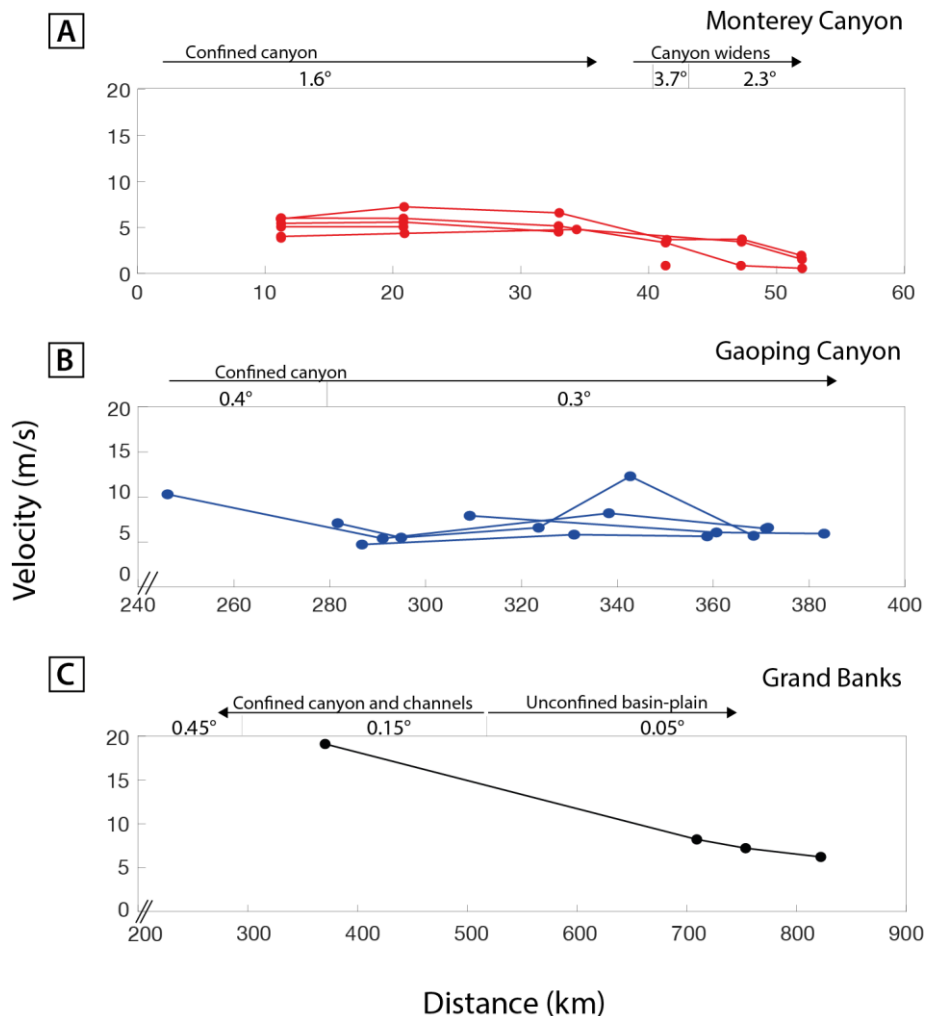


747  
 748 **Fig. 3. Velocities of turbidity currents in Monterey Canyon and properties of the thalweg.**  
 749 (A) Changes in flow velocity with distance along Monterey Canyon's thalweg. Solid dots and  
 750 solid lines show frontal velocities between moorings. Open symbols and dotted lines show  
 751 maximum internal velocity measured at each mooring by an ADCP, including for some flows  
 752 that only reached the first mooring (solid squares). (B) Changes in thalweg gradient. (C) Changes  
 753 in axial channel width, defined by the width of mapped bedforms.  
 754

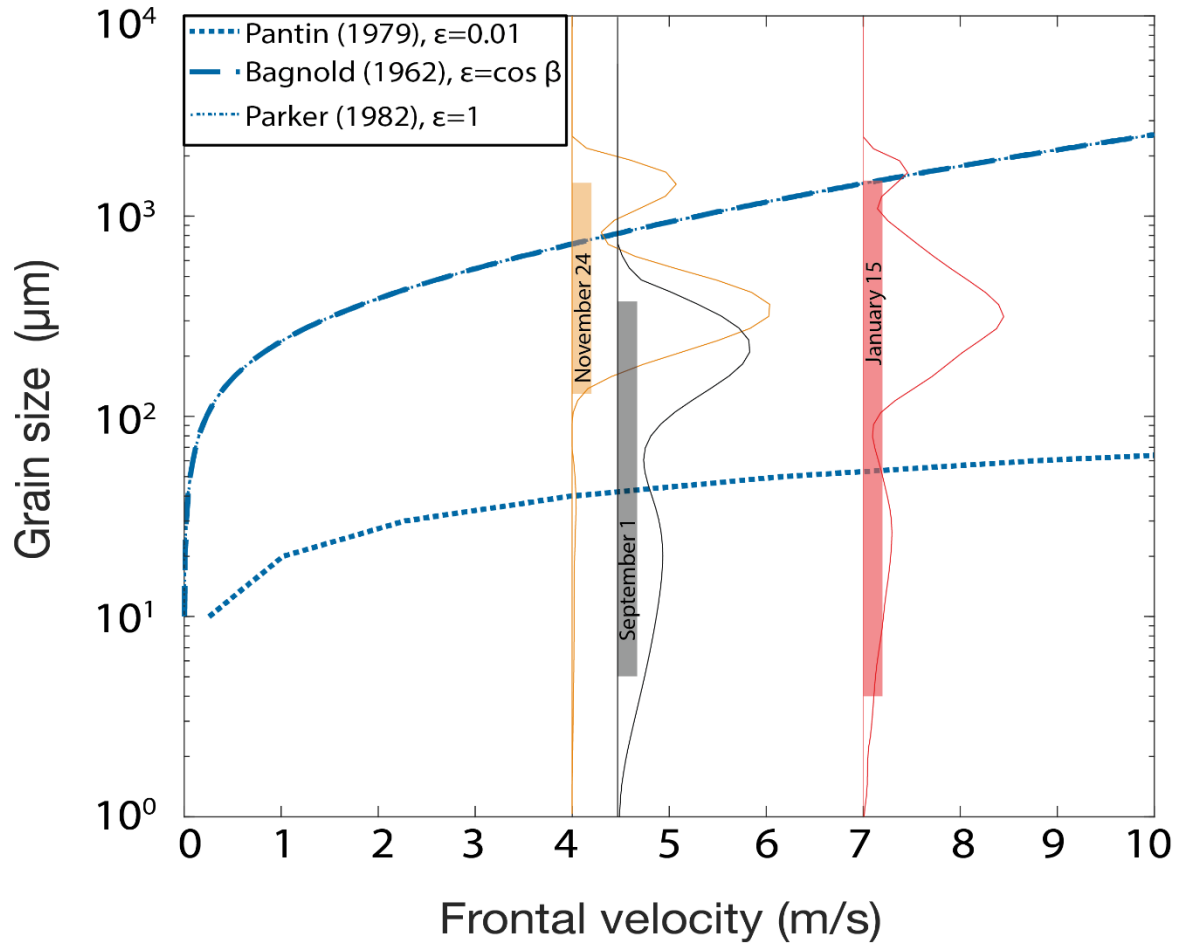
756  
757

758 **Fig. 4. Turbidity current structure at consecutive snap-shots in time, showing changes in**  
 759 **flow-length, internal velocity-structure, and flow-thickness.** Flow velocities between  
 760 moorings are inferred, as are velocities in the lower 3-4 m of the flow (due to ADCP side-lobe  
 761 interference). (A) Long run-out flow, which is initially fast, based primarily on the January 15<sup>th</sup>  
 762 event. The MS1 mooring was dragged down-canyon during the January 15<sup>th</sup> event. Thus, ADCP-  
 763 data from the February 3<sup>rd</sup> event are used for MS1 in T1 snapshot, and it is unknown if the 15<sup>th</sup>  
 764 January flow was present at MS1 during the T1+70 min snapshot. (B) Shorter runout flow that  
 765 was initially powerful, but then dissipated rapidly, based on November 24<sup>th</sup> event. This event  
 766 carried an 800 kg object at  $\geq 4$  m/s, for  $\sim 1$  km in the upper canyon (Paull et al., 2018). (C)  
 767 Example of an initially-weak turbidity current on September 1<sup>st</sup>, which then accelerated markedly  
 768 in the mid-canyon, and dissipated rapidly between MS5 and MS7. This is the only event that  
 769 occurred during summer months (Fig. 2b).

770

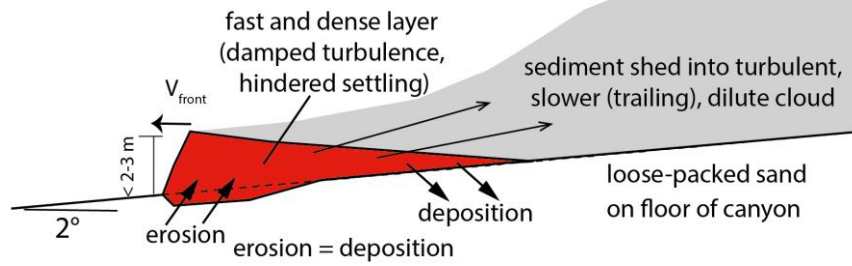


771  
 772 **Fig. 5. Changes in frontal velocities of turbidity currents over distance.** Variations in seabed  
 773 gradient and flow confinement are also shown. **(A)** Frontal velocities of flows in Monterey  
 774 Canyon. Figure 3 shows detailed changes in seabed gradient and channel floor width. **(B)** Frontal  
 775 velocities of flows confined within Gaoping Canyon, offshore Taiwan, based on cable  
 776 breaks (Gavey et al. 2017). Average seabed gradients are shown, but detailed surveys of canyon  
 777 width are currently lacking. **(C)** Frontal velocities of the Grand Banks turbidity current in 1929,  
 778 offshore Newfoundland, based on cable breaks (Heezen and Ewing, 1952; Hughes Clarke, 1988;  
 779 Piper et al., 1999). Distance is from the initial earthquake epicentre, although coincident cable  
 780 breaks occurred over a wider area. The initial part of this flow was confined by submarine fan-  
 781 valleys, but was unconfined during its later stages, as it spread across a basin plain (Piper et al.,  
 782 1999). Detailed data on the seafloor gradient over the entire length of the event are lacking, and  
 783 are based on Stevenson et al. (2018) and Piper and Hundert (2002).  
 784  
 785



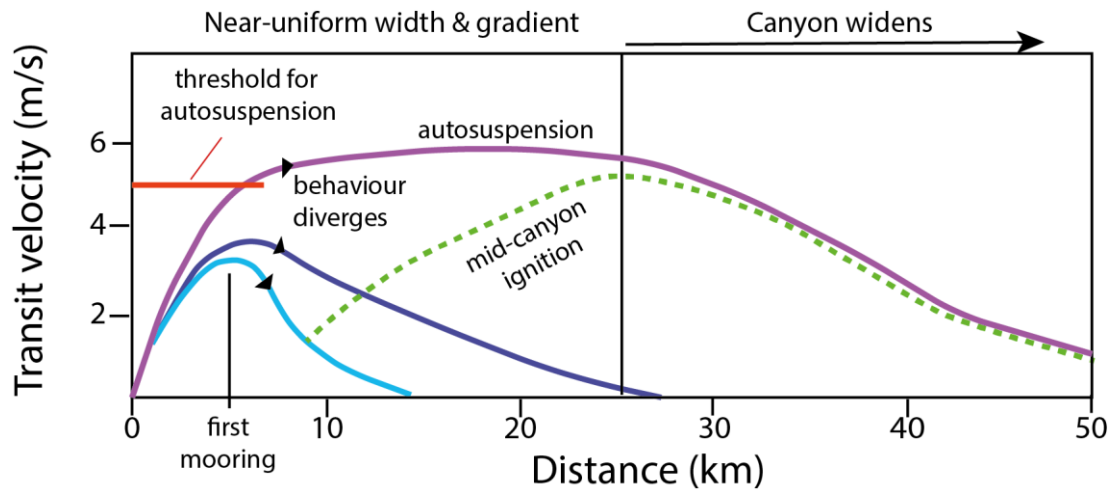
786  
 787  
 788 **Fig. 6. Comparison of field measurements in Monterey Canyon to past energy-balance**  
 789 **theory for autosuspension, following Sequeiros et al. (2009).** It shows the threshold flow  
 790 velocity predicted by three past theories, for a given grain-size and seabed gradient, above which  
 791 flows carry all suspended sediment (i.e. autosuspend). If seabed sediment is available for erosion,  
 792 the flow will also ignite. Blue lines show the different threshold constants ( $\epsilon$  in Equation 1) used  
 793 by different authors, assuming a seabed gradient of  $2^\circ$ . Autosuspension occurs below the lines.  
 794 Note that results for the threshold constant of Bagnold (1962) coincide with those of Parker  
 795 (1982) for the case of Monterey Canyon. Grain-size distributions for three events (November  
 796 24<sup>th</sup>, September, 1<sup>st</sup>, and January 15<sup>th</sup>) in Monterey Canyon, based on sediment traps located 10 m  
 797 above the bed. The grain-size distributions shown here are averages for each event in sediment  
 798 traps from the upper canyon where flows are assumed to ignite (see Material and Methodology,  
 799 Supplementary Fig. 5 for more information). The coloured boxes show the 10<sup>th</sup> percentile ( $D_{10}$ )  
 800 and 90<sup>th</sup> percentile ( $D_{90}$ ) of the coarsest grain-size samples in traps from each event.

Travelling wave model: erosive, dense frontal layer with near uniform front speed



801  
802  
803 **Fig. 7. New travelling wave model.** Travelling wave model for turbidity current behaviour in  
804 loose-sand submarine canyons, in which flows contain a fast and dense near-bed layer at their  
805 front, as proposed by (Paull et al., 2018). Erosion at the front of this dense near-bed layer is  
806 balanced by sediment deposition from its rear, leading to uniform transit velocity and  
807 autosuspension. Sediment is shed backwards to form a trailing sediment cloud that is dilute and  
808 fully turbulent, which lengthens over time.  
809





810  
 811  
 812 **Fig 8. Summarising model for turbidity current behaviour in submarine canyons underlain**  
 813 **by loose sand.** Patterns of flow behaviour, based on frontal transit velocities that are simplified  
 814 from Fig. 3a. Small increases in transit velocity at the first mooring are associated with major  
 815 differences in subsequent flow velocities and runout distance, causing divergence in flow  
 816 behaviour (purple, dark blue and light blue lines). However, flows can sometimes self-accelerate  
 817 and ignite within the mid-canyon (green dotted line), due to changes in substrate strength and  
 818 erodibility. There is a threshold initial transit velocity (red line) above which flows can  
 819 autosuspend (purple line).  
 820  
 821

822 **Table 1**

Flow Threshold	$\geq 1$ m/s							$\geq 2$ m/s							$\geq 3$ m/s						
	MS 1	MS 2	MS 3	MS 4	MS 5	SI N	MS 7	MS 1	MS 2	MS 3	MS 4	MS 5	SI N	MS 7	MS 1	MS 2	MS 3	MS 4	MS 5	SI N	MS 7
Distance (km)	6.7	16	26.0	40.0	43	51.8	52	6.7	16	26.0	40.0	43	51.8	52	6.7	16	26.0	###	43	##	52
Jan-15		87	141	182	213	112	89		9.5	59	23	41	37	22		8.5	30	0	25	0.5	0
Sep-01	20	3.5	73		22	45	0	1	0.5	7	0	11	0	0	0.5	0	0	0	3	0	0
Feb-03	48	74	73	67	65	0	0	28	17	26	0	3.5	0	0	16	15	2.5	0	0	0	0
Feb-18	34	26	70	0				15	12	16					7.5	8	1.5				
Jan-09	35	23	43					19	11	0					11	8	0				
Nov-24	33	15						12	3.5						9	0.5					
Jan-21	31							9.5							2						
Jan-20	25							7							2.5						
Dec-01	16							7							3						
Jan-23	9							0							0						
Jan-06	6.5							1							0						
Dec-11	2.5							0							0						
Jan-22				37	0						0	0						0	0		

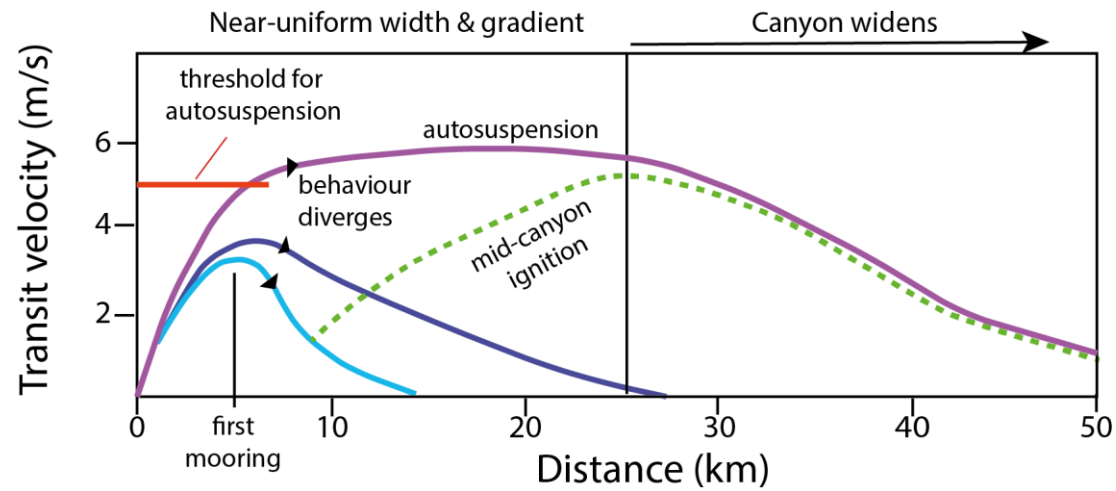
823

824 **Table 1. Flow duration (in minutes) for each mooring station and event.** For each event, a threshold flow velocity was set to determine the  
 825 duration of the flow at each mooring. The ADCP data was displayed using contour lines corresponding to each threshold, allowing for  
 826 determination of flow duration at every mooring. Left hand columns denote flow velocity threshold  $\geq 1$  m/s. Middle columns denote flow

827 velocity threshold  $\geq 2$  m/s. The right-hand column denotes flow velocity threshold  $\geq 3$  m/s. Where no flow duration is given, there was no ADCP  
828 measurement (January 15, MS1, and September 1, MS4). A duration of 0 min indicates the flow is no longer measured at the specified threshold  
829 velocity at that mooring.

830

### Graphical Abstract:



**Summarising model for turbidity current behaviour in submarine canyons underlain by loose sand.** Small increases in initial velocity cause major differences in subsequent flow velocities and runout distance, causing divergence in flow behaviour (purple, dark blue and light blue lines). However, flows can sometimes self-accelerate and ignite within the mid-canyon (green dotted line), due to changes in substrate strength and erodibility. There is a threshold initial transit velocity (red line) above which turbidity currents can autosuspend (purple line).